Prediction and simulation of battery pack usage for intelligent service robot deployment at a train station

Alexander Löwen[1], Enrique Aleman-Gallegos[2], Osarenren Kennedy Aimiyekagbon[1], Sven Wachsmuth[2], Walter Sextro[1]

[1] *Paderborn University, Chair of Dynamics and Mechatronics, Paderborn 33098, Germany*
alexander.loewen@uni-paderborn.de

[2] *Bielefeld University, Faculty of Technology, Bielefeld 33619, Germany*
jalemangallegos@techfak.uni-bielefeld.de

ABSTRACT

In order to make rail transportation more attractive compared to motorized private transport, intelligent solutions are required across the entire mobility chain. Train stations, as places of connection and transfer, offer the greatest potential in this context. Thus, the deployment of autonomous service robots at train stations offers a wide range of possibilities for supporting passengers on their journeys by rail, for example, by providing information, accompanying them to the next link in the mobility chain, or transporting their luggage. Since such robots are battery-powered, one challenge is to carefully plan activities based on the remaining battery capacity. Therefore, the aim of this work is to predict battery usage and, in turn, battery state, in order to inform passengers, and to enable intelligent planning of its usage. In this work, realistic operational conditions of a service robot are systematically assessed through measurements on the service robot itself and through passenger surveys at a train station. The estimated operational conditions are experimentally replicated to simulate the heterogeneous use of the battery pack, while acquiring condition monitoring data throughout its use. The battery pack is modeled based on the single particle model, which can robustly predict the battery state by simulating its usage considering past operational conditions. The approach is validated using experimental data obtained from simulating realistic usage. On the one hand, additional battery packs are employed, and on the other hand, the load is varied. The advantage of this approach lies in the ability to account for future changes, such as higher loads than anticipated, to provide robust predictions. This enables the intelligent use of service robots, offering passengers an improved service experience at train stations.

(a) Information service robot (b) Luggage-carrying robot

Figure 1. Service robots for the Minden train station. The (a) Temi robot and the (b) Agilex Ranger Mini V3.

1. INTRODUCTION

This work is part of the Digitaler Bahnhof Minden project which aims to enhance passenger experience in train stations by deploying two service robots, whereby Minden train station is selected as the application location. Minden train station is an important hub for long-distance and local passenger transport for the East Westphalia-Lippe region (Minden Marketing GmbH, 2023). On the one hand, the Temi robot serves as an information service robot, shown in Fig. 1a, on the other hand, the Ranger Mini robot serves as a luggage-carrying robot, shown in Fig. 1b.

The information service robot will mainly provide information to passengers relating to train departures and arrivals, providing a map of the train station to facilitate localization, and offering guidance and services at the request of passengers. On the other hand, the luggage service robot is meant to carry luggage in and around the premises of the train station.

Variable, task-dependent operation leads to inhomogeneous

battery usage and increased uncertainty in future state estimation. However, robust battery state prediction is essential to prevent mission aborts and ensure reliable autonomy. This work addresses this challenge by combining a physics-based model, specifically a single particle model (SPM), with application-specific load profiles based on real-world data to estimate remaining runtime of autonomous robots, enabling mission-level decision-making in a train station environment.

2. RELATED WORKS

Battery modeling is widely studied and encompasses circuit-based, electrochemical, and data-driven approaches. Comprehensive reviews are available, such as (Zheng et al., 2025) addressing general battery modeling. In addition, there are reviews such as (Lipu et al., 2018) that focus on methods for estimating the State of Health (SOH) and also employ probabilistic state estimation techniques such as Kalman filters.

Circuit-based approaches, such as equivalent circuit models, are particularly well-suited for battery management systems due to their computational efficiency and high accuracy (Zheng et al., 2025). They are commonly combined with Kalman filter algorithms to estimate the state of charge (SOC), as exemplary demonstrated for electric vehicles in (He et al., 2022).

Electrochemical models model the underlying electrochemical processes of battery cells. They include the SPM and the Doyle-Fuller-Newman (DFN) model. The SPM is one of the simplest physics-based models and is widely used for modeling and battery state estimation, including for estimating battery cell states in electric vehicles (Munteanu et al., 2024). It uses one spherical particle for each electrode, each described by a lithium-ion diffusion equation to reflect the behavior of the electrodes (Marquis et al., 2019). This reduction in complexity can lead to a level of efficiency capable of meeting real-time requirements, as reported in (Zheng et al., 2025). The DFN model consists of a system of strongly coupled nonlinear partial differential equations, causing the DFN model to potentially be more accurate, but also to be too computationally expensive for many applications (Marquis et al., 2019).

Data-driven methods, such as support vector machines and deep learning, have been widely applied to tasks such as SOH estimation in electric vehicles and remaining useful life prediction, as summarized in (Zheng et al., 2025) and (Lipu et al., 2018). However, data-driven methods rely highly on the availability and quality of training data.

3. RAILWAY STATION ENVIRONMENT

Fig. 2 provides an overview of the Minden train station to reveal structural properties and potential application areas for both the information service robot and the luggage-carrying robot (Bahnhofsmanagement Bielefeld, 2022).

The top view in Fig. 2a focuses on relevant structural features, including the station building with the entrance hall in the southern section. The entrance hall includes a ticket machine and a personal point of contact, while a restroom is located outside. The northern section is used to accommodate the robots during idle times and for charging. The platforms 1, 11, 12 and 13 are mainly accessible via the marked access routes from the bus stop, which is also the location of the rail replacement service.

Fig. 2b shows the areas of application for both service robots. The information service robot operates mainly in the entrance hall, whereas the luggage-carrying robot is deployed on the platforms, restricted to barrier-free paths and requiring assistance when using the lift. Relevant platform distances are determined based on train types and lengths, assuming alignment with the midline shown in Fig. 2b. An official timetable (Deutsche Bahn AG, 2024) and a railway database (Grahnert & Krings, 2026) are consulted to identify operating trains and their lengths. Platforms 11 and 13 are used for long-distance Intercity-Express (ICE) and Intercity trains, whereby the ICE 4 can reach the maximum length of up to 375 m (DB Fernverkehr AG, 2026). Considering the boundaries of the platforms are not exceeded, a relevant application range of 295 m is specified for these platforms. Platforms 1 and 12 are primarily used for local transport. However, detailed information on particular trains is not publicly available, which is why class 462 trains are used for estimation. These trains have a length of up to 157 m (Kollorz, 2024), which is defined as the relevant range for these platforms. This results in a relevant distance range for the luggage-carrying robot between about 70 m between charging station and the middle of platform 11 and about 420 m between the southern end of platform 11 and the southern end of platform 13.

4. METHODOLOGY

The proposed framework comprises 5 steps for developing and evaluating prediction models for each battery pack of the service robots.

Step 1 covers the determination of the operational conditions to examine the battery packs under realistic conditions and to design experiments for the development and evaluation of the prediction models. For the information service robot, passenger surveys and observations at the train station are considered to determine current load, frequency of use and duration of use. In contrast, the train station structure is highly relevant for the luggage-carrying robot with a focus on the load for different sections of a requested route.

In step 2, experimental investigations are conducted to reproduce the derived operational conditions through discharge cycles at defined current loads. Programmable bidirectional power supplies from Elektro-Automatik, specifically the PSB 10060-120 model, are utilized providing a nominal voltage

Figure 2. Top view of Minden train station. a) Station structure highlighting key locations: 1. Restroom, 2. Personal point of contact, 3. Ticket machine, 4. Entrance, 5–8. Platforms 1 and 11–13, 9. Parking lots, 10. Bus stop and rail replacement service; (b) Accommodation of the robots and localization of the charging stations (green), application area of the information service robot (blue) and luggage-carrying robot (red).

range of 0 to 60 V, a nominal current range of 0 to 120 A, and a power delivery capability of up to 3000 W. They offer various functionalities, including battery tests under constant current and the assignment of load profiles, utilizing up to 99 configurable curve points (EA Elektro-Automatik GmbH & Co. KG, 2022). Discharging lasts till a specified voltage is measured at the terminal. Additionally, thermocouples of type K are used in conjunction with an MCC 134 thermocouple measurement HAT on a Raspberry Pi. During experiments, the sensor tips are positioned underneath the battery packs. Sensor data is acquired at approximately 10 Hz, whereby the voltage resolution is 0.01 V and the current resolution is 0.1 A. The measurement data is processed utilizing Python. Since both the power supply control loop and the electrochemical response of the battery pack operate on time scales significantly larger than the sampling interval of 10 Hz, resampling to 5 s using time-window averaging is applied to suppress quantization-induced fluctuations that are not physically meaningful.

Step 3 addresses the first stage of model development. Since future loads may differ from current assumptions, a robust, extrapolation-capable model that relies to a limited extent on training data is preferred. The model should be capable of accurately simulating scenarios up to a certain threshold, for example, to determine the remaining runtime. Physics-based models meet these requirements, which motivated the selection of the SPM. It allows for efficient straightforward runtime simulations under specified load conditions and can be expanded in future work to account for SOH effects, while the DFN model is computationally too expensive for the considered applications. This work applies the SPM from the Python package *PyBaMM* and the Python package *liionpack* to reconstruct the battery pack of each service robot (Sulzer et al., 2021; Tranter et al., 2022). The provided parameter sets are adopted as a starting point and adjusted based on the parameters of the battery cells under investigation.

Step 4 involves the identification of relevant SPM-related parameters and optimization based on a tree-structured Parzen estimator (TPE) (Watanabe, 2023). The identification of relevant parameters is performed by simulating the discharge of the SPM for the specific cells and comparing both the discharge duration and the voltage profile with those obtained using the standard parameter values to identify parameters that influence the discharge behavior. This is done by increasing several SPM parameter values by 10 % except for constants, ambient temperature, number of electrodes connected in parallel, and electrode width, which is limited by the cell geometry. Parameters that result in a change greater than 1 % in the runtime or an R^2 score below 0.99 are optimized.

The TPE is applied to fit the model parameters to experimental data. The TPE-based optimization is chosen because it is a sample-efficient optimization approach that can effectively explore non-convex parameter spaces and handle simulation failures that may occur for unfavorable parameter combinations (Watanabe, 2023). The constraints of the previously identified parameters are set to 50 % and 150 % of their initial values. This excludes the electrode active material volume fraction, which is optimized within a physically meaningful range between 0.3 and 0.75 (Chen et al., 2020; Yuan et al., 2024). The *liionpack*-specific parameters R_b, R_c, and R_i represent resistive effects associated with the electrical interconnection of the battery cells, which are varied within a

factor of 0.1 to 10 relative to their default values. The number of initial sampling points is set to 20 times the number of varied parameters and is used to initialize the TPE optimization procedure. The total number of iterations is set to 1000. Experimental and simulated voltage curves are compared under the specified load profile.

The simulated discharge process is terminated when the terminal voltage of any series-connected cell string reaches the lower voltage cut-off defined at cell level. Due to current-dependent voltage drops and string-level heterogeneity, this criterion does not generally coincide with a fixed pack voltage compared to the experimental termination criterion. Therefore, a modified R^2 score denoted as R^2_{mod} is utilized for model evaluation during optimization which is calculated as follows. Let the measured data be given by $\{(t_i, U_i)\}_{i=1}^{N}$ and the model prediction by $\{(\tilde{t}_j, \tilde{U}_j)\}_{j=1}^{M}$, where t_i and $\tilde{t}_j$ denote the measurement and prediction time instants, respectively, and U_i and $\tilde{U}_j$ the corresponding measured and predicted voltages. The prediction is truncated as shown in Eq. (1).

$$U_{\min} = \min_i U_i, \qquad \tilde{U}_j \geq U_{\min} \tag{1}$$

Both signals are extended to the common time horizon, as derived in Eq. (2), where missing values are padded with $U_{\min}$.

$$t_{\max} = \max\left(\max_i(t_i), \max_j(\tilde{t}_j)\right) \tag{2}$$

The predicted voltage is interpolated onto the measurement time grid, yielding $\tilde{U}_i = \tilde{U}(t_i)$. Finally, the modified R^2 score is defined as formulated with Eq. (3).

$$R^2_{\mathrm{mod}} = 1 - \frac{\sum_{i=1}^{N}(U_i - \tilde{U}_i)^2}{\sum_{i=1}^{N}(U_i - \bar{U})^2}, \qquad \bar{U} = \frac{1}{N}\sum_{i=1}^{N} U_i \tag{3}$$

In step 5, realistic application scenarios are simulated and compared with experimental data to evaluate the optimized models.

5. APPLICATION EXAMPLES

The discussed methodology is applied to both the information service robot and the luggage-carrying robot separately. Operational conditions are derived and reproduced experimentally, followed by model development and evaluation.

5.1. Information Service Robot

The information service robot is equipped with a battery pack with 24 18650 cells in total. The battery pack consists of four cells connected in series per string and six such strings connected in parallel (4S6P). The battery pack has a nominal capacity of 14.70 Ah and a nominal voltage of 14.40 V. The battery pack supplies a voltage between 12.00 and 16.40 V. The robot automatically returns to the charging station at a pre-specified voltage of approximately 13.30 V (temi USA inc., 2021). The chemical composition of the cell is unknown, but its performance metrics and appearance show similarities to LCO/NMC cells available online (Ancoo Technologies (HK) Co., Limited, 2025).

The operational conditions of the information service robot are categorized into three key aspects: the type of use and its corresponding current load, the frequency of use, and the duration of use. Once these aspects are known, they can be reproduced experimentally with the power supplies utilizing load profiles.

5.1.1. Derivation of the load

The type of use is categorized into *idling*, *information*, and *navigation*. *Idling* refers to robot inactivity, such that the battery pack only powers the base load. *Information* indicates that the robot is interacting with a passenger at a stationary. *Navigation* refers to a state of movement from one position to the next, such as, to guide a passenger to the ticket machine. As the information service robot provides limited battery-related information (temi USA inc., 2023), an ESP32-based measuring device is developed to acquire and transmit measurement data via Wi-Fi. An INA260 sensor is employed to measure the current and voltage at a frequency of about 10 Hz. Additionally, a temperature sensor of type MCP9808 is placed close to the battery pack. The measuring device is stored in a cavity near the robot's battery compartment and is powered by the battery pack.

The load is determined from measurements while the information service robot interacts with people indoors and guides them in a test setting. Over a total period of about 10 min the load during *idling* is derived, over approximately 64 min during *information* and over about 259 min during *navigation*. It is observed that power consumption varies more during *navigation*, probably due to acceleration and unevenness, which is why the measurement is taken over a longer period of time. The Gaussian Kernel Density Estimation (KDE) (Virtanen et al., 2020) is applied to represent the load distribution as shown in Fig. 3. Power consumption is highest during *navigation*, reflecting the drive power required to move the robot. In contrast, power consumption during *information* deviates only slightly from the base load, suggesting that the on-board electronics account for a significant proportion of the total power consumption.

5.1.2. Derivation of the frequency of use

Passenger surveys are conducted at the train station to assess, among others, the willingness of usage and the preferred application of the information service robot. A total of 121 passengers were surveyed over three days. On the question of willingness of usage, 43.0 % of the passengers chose *yes*, 31.4 % *rather yes*, 9.9 % *rather no*, and 15.7 %

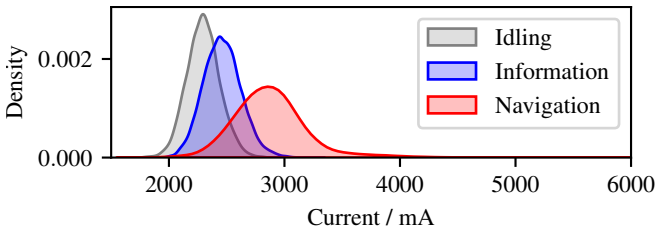

Figure 3. Gaussian Kernel Density Estimation derived from measured data for each type of use.

no. The survey indicates that the willingness to use the information service robot is high, at 74.4 % when the answers *yes* and *rather yes* are considered together. Then, passengers were asked what purpose they would use the information service robot for, when they previously answered *yes* or *rather yes*. The possible answers were *information services* such as travel information, *navigation services* such as assistance in finding locations, *other services* including entertainment through games or tourist information, and *other purposes*. Multiple selections were allowed. Of the respondents, 78 passengers (86.7 %) selected *information services*, 56 passengers (62.2 %) chose *navigation services*, 17 passengers (18.9 %) opted for *other services*, and 1 passenger (1.1 %) selected *other purposes*.

In order to derive frequencies from the survey, the percentages are normalized to the total number of responses (152). Additionally, the selections referring to *other services* as well as *other purposes* is assigned to the category *information*. This means that the information service is requested around 64 % of the time and the navigation service around 36 % of the time. Assuming that the information service robot will be idle 10.0 % of the time, this results in a distribution of usage conditions of 10.0 % *idling*, 57.6 % *information*, and 32.4 % *navigation*.

5.1.3. Derivation of the duration of use

The service points at the train station are roughly observed to estimate the duration of use for *information*, as the information service robot is supposed to accomplish similar tasks. Over a period of one hour, 7 interactions at the ticket machine and 17 at the personal point of contact were tracked to apply a Gaussian KDE. The duration is highly variable, ranging from 19 s to approximately 16 min, and the average interaction time is about 4.5 min. The same distribution is also assumed for *idling*. In order to derive the duration of use for *navigation*, distances between 1 and 60 m are considered, which is the distance between the entrance and the toilets and the longest potential distance at the train station for the information service robot. Since the average walking speed is around 1.30 m/s (Wilson & Fletcher, 2023), it is assumed for simplicity that the information service robot will move constantly at its maximum travel speed of 0.90 m/s (temi USA inc., 2021). It follows that a trip takes approximately between 1 and 67 s.

5.1.4. Experimental simulation of discharge

In order to experimentally investigate the battery pack, the load profiles are stochastically generated based on the foregoing derivations and are experimentally replicated. Hereby, a curve point of a load profile is defined in the following steps:

1. The type of use is selected with probabilities of 10.0 % for *idling*, 57.6 % for *information*, and 32.4 % for *navigation*.
2. For the *idling* and *information* cases, durations are derived from the Gaussian KDE in Section 5.1.3. In the case of *navigation*, a random value between 1 and 67 s is selected.
3. Depending on the type of use, the current is selected based on the Gaussian KDE shown in Fig. 3.

The discharge cycle is conducted until 13.30 V are measured at the terminal. Additionally, static discharge and charge cycles are conducted at 0.50 C until 12.00 V are measured at the terminal, which corresponds to the standard discharge current (Ancoo Technologies (HK) Co., Limited, 2025), mainly in order to examine the SOH in the future.

5.1.5. Model development

For model development using *PyBaMM* and *liionpack*, the predefined parameter sets by Chen et al. (Chen et al., 2020), Kim et al. (Kim et al., 2011), and O'Kane et al. (O'Kane et al., 2022) are considered. Chen et al. and O'Kane et al. investigated LG M50 cells with a graphite–silicon anode and an NMC 811 cathode, while Kim et al. derived a parameter set for lithium-ion pouch cells with a graphite anode and an NCA cathode.

Some parameters are manually set to reflect the characteristics of the cells. Specifically, electrode width and height are based on a 18650-type NMC 811 cell (Sturm et al., 2019). In addition, the open-circuit voltage (OCV) is experimentally measured, the lower voltage cut-off is set from the battery specifications, and the cell volume is derived from the specified cell dimensions (Ancoo Technologies (HK) Co., Limited, 2025). The manually set parameters with the corresponding values are listed in Table 1.

Relevant SPM-related parameters are identified by simulating a discharge cycle at 0.50 C which is a standard discharge constant current of similar battery cells (Ancoo Technologies (HK) Co., Limited, 2025) until a voltage of 3.00 V is reached. The analysis reveals that runtime is primarily affected by electrode geometry and concentration-related parameters, whereas diffusivities and particle radii have only minor influence. Using the parameter set from Chen et al., 8 parameters were identified as relevant, compared to 6 for Kim et al. and 7 for O'Kane et al.

Table 1. Manually defined PyBaMM parameters for a battery cell of the battery pack of the information service robot.

Parameter	Value	Source
Cell volume	17070.10 mm^3	a)
Electrode width	58.00 mm	b)
Electrode height	615.00 mm	b)
Lower voltage cut-off	3.00 V	c)
Nominal cell capacity	2.45 Ah	c)
Open-circuit voltage at 0 % SOC	3.18 V	d)
Open-circuit voltage at 100 % SOC	4.06 V	d)
Upper voltage cut-off	4.09 V	d)

a) Similar cell specifications (Ancoo Technologies (HK) Co., Limited, 2025).
b) Based on 18650 NMC 811 cell (Sturm et al., 2019).
c) Derived from Temi specifications (temi USA inc., 2021).
d) Experimentally measured considering the battery pack configuration.

Table 2. Optimization results based on the R^2_{mod} score.

Opt. profile	Parameter Set	Opt. Result	Val. Result
Dynamic	**Chen et al.***	**0.97**	**0.95**
Dynamic	Kim et al.*	0.55	−0.61
Dynamic	O'Kane et al.*	0.98	0.93
Static	Chen et al.*	0.97	0.94
Static	Kim et al.*	−0.51	0.55
Static	O'Kane et al.*	0.97	0.92

*(Chen et al., 2020; Kim et al., 2011; O'Kane et al., 2022)

The numerical model is optimized based on the static discharge profile and validated based on the dynamic discharge profile, and vice versa. The optimization converges quickly to a plateau after the initialization phase and subsequently varies around it at each iteration. The results are summarized in Table 2. Among the considered parameter sets, the model based on Chen et al. achieves the highest validation results for both profiles. In the following, the model, adapted to the dynamic discharge profile, is used. The simulations of the static and dynamic discharge profile are shown in Fig. 4, where the simulation result is truncated as specified in Eq. (1). Over the full dynamic discharge cycle, discrepancies become apparent around 120 and 250 min. At the same time, the model exhibits a high degree of accuracy at the beginning and in the range of approximately 150 min and 230 min. The optimized parameter values are listed in Table 3. Some parameters, particularly the cathode volume fraction, deviate from typical NMC cell values, suggesting compensatory effects and limited identifiability of the parameters. For the most part, however, the parameters appear to be physically plausible.

The strategy for predicting the runtime after any period of service comprises the following steps:

1. Calibrate the SOC of the numerical model using the most recent measurement of current, voltage and temperature by performing short simulations.
2. Simulate the battery pack's operation under the average current of the present discharge cycle at the lastly measured temperature.
3. Determination of the time elapsed until 13.30 V are measured.

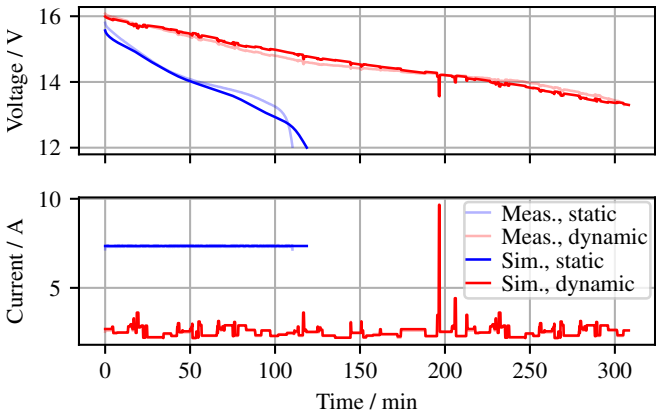

Figure 4. Optimized numeric model of the battery pack of the information service robot applied on the static and dynamic discharge profile, where the model is adapted to the dynamic discharge profile with respect to the voltage profile.

Table 3. Optimized parameters for the battery pack of the information service robot.

Parameter	Value
Electrode height	897.19 mm
Initial concentration in neg. electrode	27413.85 $\mathrm{mol\,m^{-3}}$
Initial concentration in pos. electrode	23931.38 $\mathrm{mol\,m^{-3}}$
Max. concentration in pos. electrode	84931.99 $\mathrm{mol\,m^{-3}}$
Neg. electrode active material volume fraction	0.71
Neg. electrode thickness	121.37 μm
Pos. electrode active material volume fraction	0.36
Pos. electrode thickness	110.49 μm
R_{b}	0.53 $m\Omega$
R_{c}	98.29 $m\Omega$
R_{i}	36.42 $m\Omega$

5.1.6. Model evaluation

Four experimental dynamic discharge profiles are considered, each of which originates from different battery packs of the information service robot. In stages, after runtimes of 30, 60, ..., 300 min, the task is to estimate the remaining runtime by applying the presented strategy. The actual remaining runtime is compared to the simulated runtime. The results are presented in Fig. 5. Notably, battery pack 1 corresponds to the pack used in the model development. The weakness previously identified is apparent in the evaluation at around after 150 min runtime, but is compensated towards the end. The mean absolute error (MAE) is 14.92 min and the mean absolute percentage error (MAPE) is 18.88 %.

5.2. Luggage Service Robot

The luggage-carrying robot is powered by a battery pack with a 15S4P configuration which provides a voltage in the range 45.00 to 54.00 V. The battery pack is rated at 48.00 V and 24.00 Ah. It is stated that LiFePO4 cells are employed and the powertrain is shut down at 10 % SOC (AgileX Robotics Team, 2024). The dimensions are consistent with cylindri-

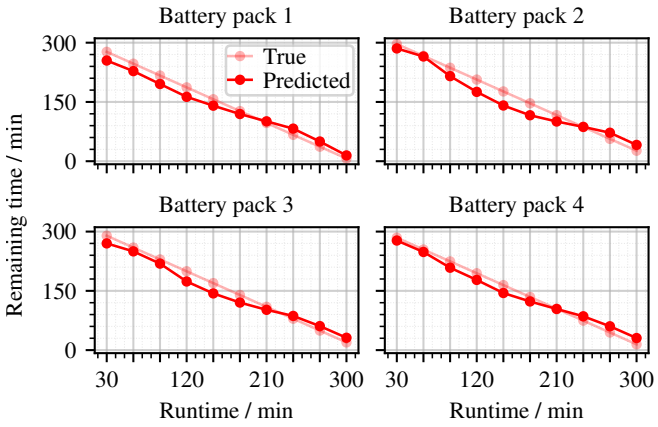

Figure 5. Evaluation of the numerical model after specified experimental runtimes on four discharge cycles of four different physical battery packs.

cal 32700 cells and are visually and technically similar to 32700 LiFePo4 cells that are available online (EVLithium Limited, 2025). Battery-related data, such as current, voltage and SOC, can be retrieved from the robot using its SDK (AgileX Robotics (Dongguan) CO,.ltd, 2025). At 10 % SOC, an average voltage of 46.31 V at an average discharge current of 1.70 A is measured during standstill.

The passenger survey reveals that the preferred frequency of use of the luggage service robot with 81.3 % is irregular, e.g., for vacations. For this reason, the focus is on the request itself and, consequently, on the route being requested. The key aspects that need to be quantified are the load and distance of a route and, accordingly, the duration, whereby the distances are already specified in Section 3. It is assumed that the luggage-carrying robot is waiting for a job at the battery charging station and will return there once the task is completed. The goal is then to determine whether or not the robot can accept the task based on its charge level.

5.2.1. Derivation of the load

Unlike the information service robot, the luggage-carrying robot has the ability to measure necessary battery-related data and provide it remotely via its SDK. Battery-related information is collected under various load conditions on a test track at CITEC in Bielefeld, which consists of an estimated 18 m of flat terrain and a slope of about 17 m to consider the slopes of the no-barrier paths at the train station. The tests are conducted 3 cycles with no load and with loads of 20, 40, 60, and 80 kg at the maximum speed of 0.50 m/s for autonomous driving. Analogous to Temi, Gaussian KDE is applied to determine the load distribution per payload and slope, totaling 15 distributions. Fig. 6 exemplarily shows the distribution of the case with 80 kg of payload. The current varies depending on the load and slope. Occasional low and high currents can occur when driving over bumps and small stones leading to a minimum current of approximately 0.50 A and a maximum current of 7.30 A measured. During standstill, the current is approximately 1.70 A.

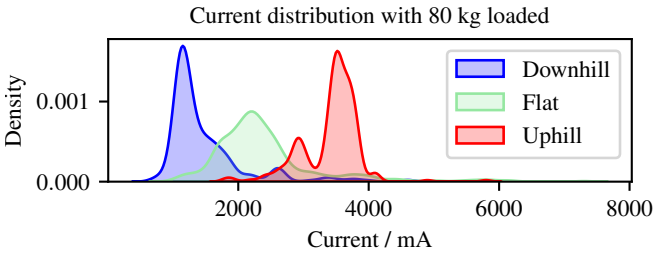

Figure 6. Gaussian Kernel Density Estimation derived from the test track at CITEC in Bielefeld with 80 kg of payload.

5.2.2. Experimental simulation of discharge

The luggage-carrying robot experiences a wider range and variation of loads, influenced by both payload and travel path. Taking this into account in the design of the numerical model, an experiment is conducted in which stepwise currents of 0.5, 1, 2, ..., 8 A are applied, each for a duration of 10 min until 45.00 V is measured at the terminal. This experiment serves as the basis for adapting the numerical model.

The load profiles for the experiments are exemplarily based on the reconstruction of the longest possible route, which is approximately 420 m between the southern end of platform 11 and the southern end of platform 13, where it carries the luggage of the passenger. Considering the charging station as starting and ending point, this results in an additional 190 m between the charging station and the southern end of platform 11, as well as 280 m between the southern end of platform 13 and the charging station. The route includes 75 m of both uphill and downhill terrain. At a constant travel speed of 0.50 m/s, this corresponds to a total travel time of 29.67 min. In addition, 2 min are exemplarily included for loading and unloading during standstill. The load profile is generated in the following steps, whereby the currents are obtained from the Gaussian KDE derived in Section. 5.2.1 and the duration specified in a curve point is approximately 19 s unless otherwise specified:

1. Simulation of a 60 s standstill at 1.70 A (one curve point).
2. Simulation of the path from charging station to platform 11 with a total of 380 s of driving on flat terrain without load.
3. Simulation of the path from platform 11 to platform 13 with a total of 690 s of driving on flat terrain and 150 s on uphill terrain with load.
4. Simulation of the path from platform 13 to charging station with a total of 410 s of driving on flat terrain and 150 s on downhill terrain without load.
5. Simulation of a 60 s standstill at 1.70 A (one curve point).

This results in a total of 97 curve points and enables a large

Table 4. Manually defined PyBaMM parameters for a battery cell of the luggage-carrying robot battery pack.

Parameter	Value	Source
Cell volume	$57410.40\,\mathrm{mm}^3$	a)
Electrode width	$70.20\,\mathrm{mm}$	a)
Electrode height	$6837.61\,\mathrm{mm}$	a), b)
Lower voltage cut-off	$3.00\,\mathrm{V}$	c)
Nominal cell capacity	$6.00\,\mathrm{Ah}$	c)
Open-circuit voltage at 0 % SOC	$3.18\,\mathrm{V}$	d)
Open-circuit voltage at 100 % SOC	$3.33\,\mathrm{V}$	d)
Upper voltage cut-off	$3.62\,\mathrm{V}$	d)

a) Similar cell specifications (EVLithium Limited, 2025).
b) $LiFePO_4$ specification sheet (NEI Corporation, 2024).
c) Derived from Ranger Mini specifications (AgileX Robotics Team, 2024).
d) Experimentally measured considering the battery pack configuration.

variation to be realized with one load profile, which takes in sum 31.67 min.

5.2.3. Model development

The $LiFePO_4$–graphite parameter set is derived from Prada et al. (Prada et al., 2013), as it is currently the only one implemented in the *PyBaMM* framework. As before, some parameters are manually specified. The electrode height is calculated from the nominal cell capacity, the areal capacity of the positive electrode, which is estimated to be 1.25 mAh/cm^2 (NEI Corporation, 2024), and the estimated electrode width of 70.20 mm, resulting in an electrode height of 6837.60 mm. The set parameters are given in Table 4.

The identification of relevant SPM-related parameters reveals that geometric and positive electrode parameters dominate the runtime behavior, whereas parameters related to the negative electrode have only marginal influence. 10 parameters are identified as relevant. The optimization procedure applied to the stepped experiment leading to an R^2_{mod} score of 0.98. The result is presented in Fig. 7. The optimized parameter values are listed in Table 5. Also here, some parameter combinations indicate compensation effects, such as the combination of a thin negative electrode and a high fraction of its active material volume. Since the individual parameter values appear physically plausible and the focus is on an accurate representation of battery behavior, the optimized model is used in the following.

5.2.4. Model Evaluation

For evaluation, the longest possible route is experimentally emulated twice in succession, as described in Section 5.2.2, aiming to complete the second cycle just before the battery reaches a voltage of 46.31 V at a load current of 1.70 A. Although the luggage-carrying robot triggers shutdown based on SOC, the evaluation is consistently performed using the voltage threshold, as for the information service robot. This ensures comparability, as voltage is directly measurable. Consequently, no request may be accepted if it would cause the voltage to fall below 46.31 V at 1.70 A.

Table 5. Optimized parameters for the battery pack of the luggage-carrying robot.

Parameter	Value
Electrode height	$8899.80\,\mathrm{mm}$
Initial concentration in neg. electrode	$36876.97\,\mathrm{mol\,m^{-3}}$
Max. concentration in neg. electrode	$39754.21\,\mathrm{mol\,m^{-3}}$
Max. concentration in pos. electrode	$30909.19\,\mathrm{mol\,m^{-3}}$
Neg. electrode active material volume fraction	0.66
Neg. electrode thickness	$17.01\,\mu\mathrm{m}$
Pos. electrode active material volume fraction	0.35
Pos. electrode thickness	$114.62\,\mu\mathrm{m}$
Pos. particle diffusivity	$6.43 \times 10^{-18}\,\mathrm{m^2\,s^{-1}}$
Pos. particle radius	$0.06\,\mu\mathrm{m}$
R_{b}	$0.42\,m\Omega$
R_{c}	$8.78\,m\Omega$
R_{i}	$97.84\,m\Omega$

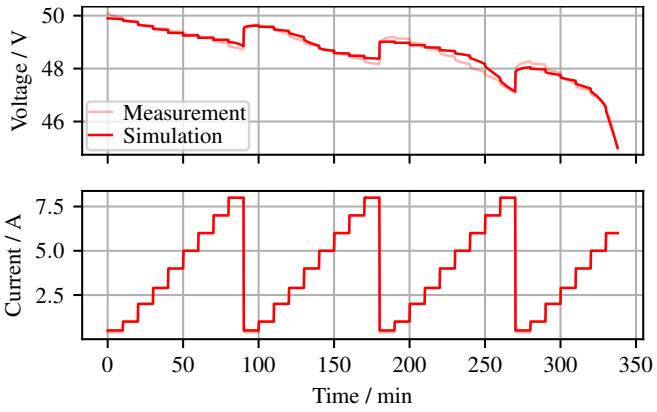

Figure 7. Optimized numeric model of the battery pack of the luggage-carrying robot with respect to the voltage profile.

The objective is to predict the voltage at 1.70 A after completion of a single cycle. This involves simulating the route using average loads for the route sections gathered in Section 5.2.1. The evaluation is conducted on 3 different battery packs, with one result shown as an example in Fig. 8, for payloads of 20, 40, 60, and 80 kg. The voltage after the first cycle is slightly overestimated, whereas it is underestimated after the second cycle. The underestimation is conservative and therefore preferable, as it provides a safety margin to account for uncertainties in real-world operation. The cases show comparable accuracy, where the MAE ranges between approximately 0.15 and 0.22 V and the MAPE remains below 0.5 %. Overall, the average MAE is 0.17 V and the average MAPE is 0.37 %.

6. CONCLUSION

This work presents a physics-based framework for runtime and route feasibility prediction of service robots, an information service robot and a luggage-carrying robot, using a SPM for intelligent service robot deployment at a train station. Task- as well as route-specific load profiles are derived from local structural conditions, passenger surveys, and ex-

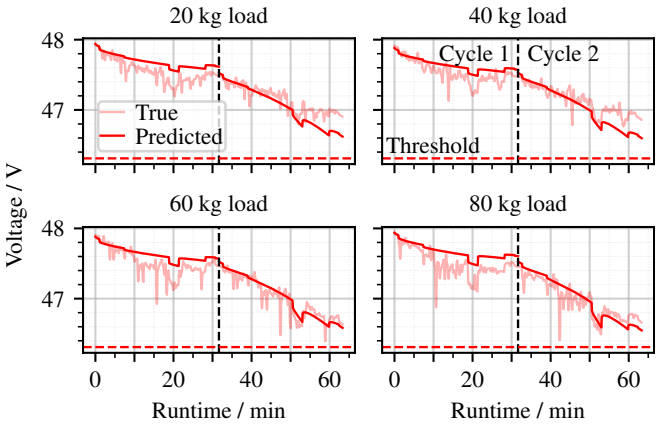

Figure 8. Evaluation of the numerical model for two sequential cycles with 20, 40, 60, and 80 kg of load.

perimental measurements on the robots. SPM parameters and pack-level resistance parameters are optimized for each robot using experimental discharge curves with respect to the measured voltage profiles.

The derived load profiles are experimentally emulated to validate the prediction strategy. For the information service robot, the objective is to predict the remaining runtime. Averaged over four distinct battery packs and corresponding load profiles, the model achieves a MAE of 14.92 min and a MAPE of 18.88 %. For the luggage-carrying robot, the objective is to estimate the battery pack voltage after completion of a luggage transport task in order to determine whether the requested task can be accepted. When emulating the longest route with four different payloads at two different starting voltages, the model achieves a MAE of 0.17 V and a MAPE of 0.37 % on average. The results highlight the feasibility of physics-based modeling for complete battery packs in practical robotic applications, enabling reliable mission-level decision support.

Future work will address the compensation effects that arose during the optimization process by introducing additional constraints to ensure more plausible parameter combinations. The battery models will be integrated into decision-making frameworks to further enhance robotic autonomy. For the information service robot, the predictive model will be extended to support interactive operation scenarios in which the robot estimates its remaining energy budget and autonomously selects or communicates a set of feasible tasks based on the predicted runtime. With regard to the luggage-carrying robot, active route planning will be incorporated, building on previous work (Lian Sang et al., 2025). This will replace the current database-based evaluation of predefined routes and enable dynamic route assessment based on real-time position, increasing the flexibility of the proposed prediction strategy.

ACKNOWLEDGMENT

Special thanks to Liwen Hou, who conducted the survey at the train station as part of her bachelor's thesis.

This work was supported by the EFRE/JTF program NRW *REGIONALE Ostwestfalen-Lippe – Networked Mobility and Digital Applications*. Project: *Digitaler Bahnhof Minden (DiBaMi)* # 34.EFRE-20300000.

Kofinanziert von der Europäischen Union

Ministerium für Umwelt, Naturschutz und Verkehr des Landes Nordrhein-Westfalen

REFERENCES

AgileX Robotics (Dongguan) CO,.ltd. (2025). *Ugv sdk.* https://github.com/agilexrobotics/ugv_sdk. (Accessed: 2025-12-23)

AgileX Robotics Team. (2024). *Ranger mini 3.0 user manual.* https://static.generation-robots.com/media/ranger-mini-mini-3.0-user-manual.pdf. (Accessed: 2026-01-08)

Ancoo Technologies (HK) Co., Limited. (2025). *Lishen LS LR1865SK LCO/NCM 18650 Li-ion cell Specifications.* https://www.ancoo-battery.com/en/product/LR1865SK.html. (Accessed: 2025-12-23)

Bahnhofsmanagement Bielefeld. (2022). *Umgebungsplan: Minden (westf).* https://www.bahnhof.de/downloads/replacement-service-maps/4120.pdf. (Accessed: 2026-01-07)

Chen, C.-H., Planella, F. B., O'Regan, K., Gastol, D., Widanage, W. D., & Kendrick, E. (2020). Development of experimental techniques for parameterization of multi-scale lithium-ion battery models. *Journal of The Electrochemical Society*, *167*(8), 080534. doi: 10.1149/1945-7111/ab9050

DB Fernverkehr AG. (2026). *ICE 4.* https://www.bahn.de/service/ueber-uns/zugtypen/ice-4. (Accessed: 2026-01-07)

Deutsche Bahn AG. (2024). *Regeltafel Minden (Westf).* https://www.bahnhof.de/minden-westf/fahrplan. (Accessed: 2025-01-09)

EA Elektro-Automatik GmbH & Co. KG. (2022). *Handbuch EA-PSB 10000 2U: Programmierbare bidirektionale DC-Netzgeräte* (User manual).

EVLithium Limited. (2025). *32700 lifepo$_4$ battery cell: 3.2 v 6000 mah cylindrical cell.* https://www.evlithium.com/hot-lithium-battery/32650-32700-lifepo4-battery-cell.html. (Accessed: 2026-1-13)

Grahnert, M., & Krings, M. (2026). *Datenbank Fernverkehr.* https://www.fernbahn.de/

datenbank/suche/. (Accessed: 2026-01-07)

He, J., Meng, S., & Yan, F. (2022). A comparative study of soc estimation based on equivalent circuit models. *Frontiers in Energy Research*, *Volume 10 - 2022*. doi: 10.3389/fenrg.2022.914291

Kim, G.-H., Smith, K., Lee, K.-J., Santhanagopalan, S., & Pesaran, A. (2011). Multi-domain modeling of lithium-ion batteries encompassing multi-physics in varied length scales. *Journal of The Electrochemical Society*, *158*(8), A955–A969. doi: 10.1149/1.3597614

Kollorz, W. (2024). *Die Fahrzeuge im Regionalverkehr.* https://www.nahverkehr-franken.de/rbahn/462-techdat.html. (Accessed: 2026-01-07)

Lian Sang, C., Drawe, M., Siekmann, T., Hesse, M., & Rückert, U. (2025). Public 5G-Aided Robust Smartphone GNSS Localization in Challenging Environments. In *2025 ieee future networks world forum (fnwf)* (pp. 1–6). IEEE. doi: 10.1109/FNWF66845.2025.11317753

Lipu, M. H., Hannan, M., Hussain, A., Hoque, M., Ker, P. J., Saad, M., & Ayob, A. (2018). A review of state of health and remaining useful life estimation methods for lithium-ion battery in electric vehicles: Challenges and recommendations. *Journal of Cleaner Production*, *205*, 115-133. doi: https://doi.org/10.1016/j.jclepro.2018.09.065

Marquis, S. G., Sulzer, V., Timms, R., Please, C. P., & Chapman, S. J. (2019). *An asymptotic derivation of a single particle model with electrolyte.* Retrieved from https://arxiv.org/abs/1905.12553

Minden Marketing GmbH. (2023). *Rechtes Weserufer.* https://www.minden-erleben.de/tourismus/index.php/de/?option=com_content&view=article&id=1855&catid=501&lang=de-DE. (Accessed: 2026-01-07)

Munteanu, I., Bratcu, A. I., Thivel, P.-X., Bultel, Y., Georges, D., & Decaux, C. (2024). Single-particle model of li-ion battery – model calibration and validation against real data in an electric vehicular application. *IFAC-PapersOnLine*, *58*(13), 23-30. (12th IFAC Symposium on Control of Power and Energy Systems - CPES 2024) doi: https://doi.org/10.1016/j.ifacol.2024.07.454

NEI Corporation. (2024). *Nanomyte® be-60e $LiFePO_4$ specification sheet.* https://www.neicorporation.com/specs/NANOMYTE_BE-60E_LFP_Spec_Sheet.pdf. (Accessed: 2026-1-13)

O'Kane, S. E. J., Ai, W., Madabattula, G., Alonso-Alvarez, D., Timms, R., Sulzer, V., … Marinescu, M. (2022). Lithium-ion battery degradation: How to model it. *Physical Chemistry Chemical Physics*, *24*, 7909–7922. doi: 10.1039/D2CP00417H

Prada, E., Domenico, D. D., Creff, Y., Bernard, J., Sauvant-Moynot, V., & Huet, F. (2013). A simplified electrochemical and thermal aging model of $LiFePO_4$-graphite li-ion batteries: Power and capacity fade simulations. *Journal of The Electrochemical Society*, *160*(4), A616–A628. doi: 10.1149/2.053304jes

Sturm, J., Rheinfeld, A., Zilberman, I., Spingler, F., Kosch, S., Frie, F., & Jossen, A. (2019). Modeling and simulation of inhomogeneities in a 18650 nickel-rich, silicon-graphite lithium-ion cell during fast charging. *Journal of Power Sources*, *412*, 204-223. doi: https://doi.org/10.1016/j.jpowsour.2018.11.043

Sulzer, V., Marquis, S. G., Timms, R., Robinson, M., & Chapman, S. J. (2021). Python Battery Mathematical Modelling (PyBaMM). *Journal of Open Research Software*, *9*(1), 14. doi: 10.5334/jors.309

temi USA inc. (2021). *temi: The personal robot, s1 technical spec, revision-09* (Tech. Rep.). Robotemi Ltd. (Technical Specifications)

temi USA inc. (2023). *temi sdk.* https://github.com/robotemi/sdk. (Accessed: 2025-12-22)

Tranter, T. G., Timms, R., Sulzer, V., Planella, F. B., Wiggins, G. M., Karra, S. V., … Brett, D. J. l. (2022). liionpack: A python package for simulating packs of batteries with pybamm. *Journal of Open Source Software*, *7*(70), 4051. doi: 10.21105/joss.04051

Virtanen, P., Gommers, R., Oliphant, T. E., Haberland, M., Reddy, T., Cournapeau, D., … SciPy 1.0 Contributors (2020). SciPy 1.0: Fundamental Algorithms for Scientific Computing in Python. *Nature Methods*, *17*, 261–272. doi: 10.1038/s41592-019-0686-2

Watanabe, S. (2023). Tree-structured Parzen estimator: Understanding its algorithm components and their roles for better empirical performance. In *arxiv:2304.11127*.

Wilson, D. R., & Fletcher, J. (2023). *What is the average walking speed?* https://www.medicalnewstoday.com/articles/average-walking-speed. (Accessed: 2025-05-06)

Yuan, X.-D., Xiong, Z.-K., Li, L.-C., Tang, C.-Y., Jia, Q.-W., Tuo, H.-C., & Zhang, Y. (2024). Study on the effects of electrode volume fraction and electrode particle radius on dynamic electrochemical-thermal-aging coupling characteristics of lithium cell based on cylindrical cell design method. *Chemical Engineering Journal*, *499*, 156204. doi: https://doi.org/10.1016/j.cej.2024.156204

Zheng, B., Deng, Z., Luo, Z., Mao, S., Ouyang, M., Han, X., … Zhu, Y. (2025). A comprehensive review of lithium-ion battery modelling research and prospects: in-depth analysis of current research and future directions. *Applied Energy*, *401*, 126688. doi: https://doi.org/10.1016/j.apenergy.2025.126688